

## Accepted Manuscript

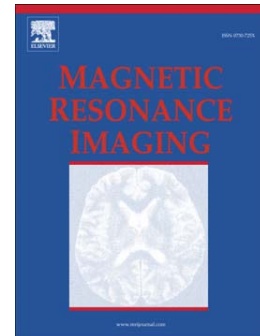
Distance Regularized Two Level Sets for Segmentation of Left and Right Ventricles from Cine-MRI

Yu Liu, Gabriella Captur, James C. Moon, Shuxu Guo, Xiaoping Yang, Shaoxiang Zhang, Chunming Limy

PII: S0730-725X(15)00322-7  
DOI: doi: [10.1016/j.mri.2015.12.027](https://doi.org/10.1016/j.mri.2015.12.027)  
Reference: MRI 8491

To appear in: *Magnetic Resonance Imaging*

Received date: 19 November 2015  
Accepted date: 14 December 2015



Please cite this article as: Liu Yu, Captur Gabriella, Moon James C., Guo Shuxu, Yang Xiaoping, Zhang Shaoxiang, Limy Chunming, Distance Regularized Two Level Sets for Segmentation of Left and Right Ventricles from Cine-MRI, *Magnetic Resonance Imaging* (2015), doi: [10.1016/j.mri.2015.12.027](https://doi.org/10.1016/j.mri.2015.12.027)

This is a PDF file of an unedited manuscript that has been accepted for publication. As a service to our customers we are providing this early version of the manuscript. The manuscript will undergo copyediting, typesetting, and review of the resulting proof before it is published in its final form. Please note that during the production process errors may be discovered which could affect the content, and all legal disclaimers that apply to the journal pertain.

## Distance Regularized Two Level Sets for Segmentation of Left and Right Ventricles from Cine-MRI

Sun Dec 27 01:08:03 2015

Yu Liu<sup>a</sup>; Gabriella Captur<sup>b,c</sup>; James C Moon<sup>b,c</sup>; Shuxu Guo<sup>a</sup>; Xiaoping Yang<sup>d</sup>; Shaoxiang Zhang<sup>e,\*\*</sup>; Chunming Limy<sup>f,\*</sup>

<sup>a</sup>College of Electronic Science and Engineering, Jilin University, Changchun, P.R.China

<sup>b</sup>Institute of Cardiovascular Science, University College London, London, United Kingdom

<sup>c</sup>The Barts Heart Centre, St Bartholomew's Hospital, Barts Health NHS Trust, London, United Kingdom

<sup>d</sup>School of Science, Nanjing University of Science and Technology, Nanjing, P. R. China

<sup>e</sup>Institute of Digital Medicine, Third Military Medical University (TMMU), Chongqing, P.R.China

<sup>f</sup>School of Electronic Engineering, University of Electronic Science and Technology of China(UESTC), Chengdu, P.R. China

\*Co-corresponding author, email:chunming.li@uestc.edu.cn

\*\*Co-corresponding author, email:zhangcvh@aliyun.com

### Abstract

This paper presents a new level set method for segmentation of cardiac left and right ventricles. We extend the edge based distance regularized level set evolution (DRLSE) model in [18] to a two-level-set formulation, with the 0-level set and  $k$ -level set representing the endocardium and epicardium, respectively. The extraction of endocardium and epicardium is obtained as a result of the interactive curve evolution of the 0 and  $k$  level sets derived from the proposed variational level set formulation. The initialization of the level set function in the proposed two-level-set DRLSE model is generated from roughly located endocardium, which can be performed by applying the original DRLSE model. Experimental results have demonstrated the effectiveness of the proposed two-level-set DRLSE model.

Keywords: MRI, segmentation, two-level-set, left and right ventricles

## 1 Introduction

Cine-magnetic resonance imaging (cine-MRI) has become a crucial tool for evaluating heart size and function within the cardiovascular imaging domain. The typical acquisition consists of a set of multiphase two-dimensional steady-state free precession short axis images, forming the 'cine stack'. Cine-MRI-derived metrics like left and right ventricular (LV, RV) volumes, mass and ejection fraction (EF) are fundamental to cardiology: clinically they are used for disease diagnosis, to guide risk stratification and therapy decisions and increasingly in research, they are serving as surrogate end-points in large-scale phase III clinical trials. Segmentation of the ventricular chambers is necessary to extract these values for ventricular size, mass and function [19], [28], [29], [40], [16], [32], [9], [27], [7]. Manual segmentation of LV and RV which requires delineation via physicians and radiologists slice by slice is a time consuming and error-prone task. This approach is simply not feasible for the analysis of large cine-MRI datasets such as the ones currently collecting in large multi-centre registries/biobanks such as the UK Biobank [8], Multi-Ethnic Study of Atherosclerosis [34] or the EuroCMR registry [3]. Although various automated/semi-automated segmentation techniques have been proposed, fast, accurate and precise, LV and RV segmentation remains a challenge largely on account of suboptimal image contrast across the desired ventricle boundaries and the difficulties related to partial volume effects towards the apex [29], [9], [30], [21], [41], [1], [42], [23], [10].

Active contour models and level set methods have been widely implemented to segment various biological structures in biomedical imaging [4], [31], [14], [22]. Active contour models have several desirable advantages when compared to other classical image segmentation methods, such as visual thresholding, edge-detection and region-grow. Firstly, active contour models are capable of achieving sub-pixel accuracy of object boundaries. Secondly, these models can be easily formulated into a principled energy minimization framework, facilitating the incorporation of prior knowledge like shape or intensity distribution, for robust image segmentation [5], [17]. Thirdly, active contour models can provide smooth and closed contours as segmentation outcomes which are key to segmenting most biological structures and can be readily used for further applications, such as shape analysis and image reconstruction [39], [37], [38], [26], [25], [24].

In order to segment the endocardial and epicardial contours of both ventricles from cine-MRI, we propose a two-level-set approach based on the DRLSE model in [18]. In this new method, endocardial and epicardial contours are mathematically represented by two specified level contours of a level set function. Biventricular segmentation is expressed as an optimization problem of the level set function such that both level set contours best capture the biological shape of epicardium and endocardium.

The paper is further structured as follows: Section 2 describes the details of proposed algorithm, Section 3 proposes a two-step approach for segmentation of left and right ventricles and Section 4 presents the implementation details as well as segmentation results, which is followed by the concluding remarks in Section 5.

## 2 Distance Regularized Two-Level-Set Method

### 2.1 Anatomical Knowledge for Left and Right Ventricle Segmentation

As a first step we have to consider the anatomy of both ventricles to be able to develop the proposed model. As presented in Figure 1, the endocardium represents the innermost contour of the ventricle. It is composed of a thin layer of endocardial cells (similar to the endothelial cells that line vessel walls). The endocardium is not a naturally smooth contour but a complex three-dimensional surface - it is continuous with the intricate trabecular meshwork that lines the heart and it extends to line the papillary muscles. The myocardium is the thick middle layer composed of cardiomyocytes. It is the force-generating muscle layer, responsible for ejecting the stroke volume. The outer layer of heart is termed the epicardium and it consists of flattened epithelial cells making up the inner serous layer of the pericardium [29], [12].

Based on several informative observations of cardiac anatomy and given that endocardial segmentation has been shown to be most reproducible with trabeculae/papillary muscles excluded [11], we concluded that the desired segmentation outputs should fulfill the following two criteria: first, that the endocardial and epicardial contours should consist of smooth contours, and second, that the interval between endocardial and epicardial contours should vary smoothly. For the developed segmentation method to be clinically valid, it would also need to demonstrate highly reproducible. Figure 1 demonstrates a typical example of the desired LV and RV segmentation results which satisfy the two predefined criteria. These criteria will be incorporated into the formulation of proposed model for LV and RV segmentation. In particular, the first criterion will be introduced to smooth the epicardial and endocardial contours individually, while the second criterion will be introduced to provide an interaction between the two contours such that the distance between them is gradually varying.

Figure 1 shows one short-axis cine-MRI image at end-diastole and end-systole. It is immediately evident that the left and right ventricular cavities show brighter signal intensity when compared to surrounding tissues, including the myocardium, papillary muscles and trabeculae and more peripherally, the lung parenchyma or anterior chest wall. Papillary muscles and trabeculae have an intensity value very similar to that of the myocardium [15], [35]. If papillary muscles and trabeculae are included in the segmentation detail, then the resulting endocardial contour cannot be smooth and accordingly, the distance between the endocardial and epicardial contours will fluctuate significantly. This undesirable segmentation result can be avoided by maintaining the two predefined criteria of endocardial and epicardial contours.

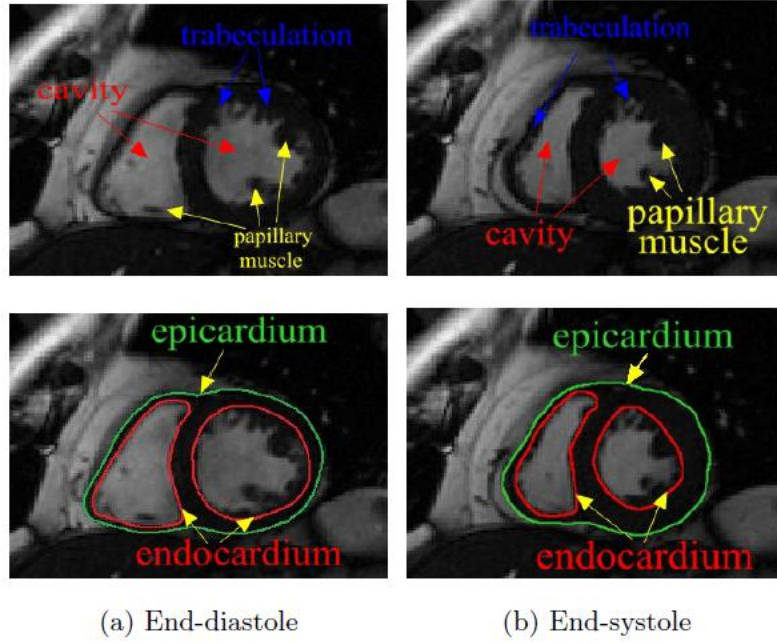


Figure 1: Short axis cine-MRI view of one representative patient at end-diastole (left column) and end-systole (right column) respectively, including the anatomical explanation of both left and right ventricles (top row) as well as the desired epicardial contours (green) and endocardial contours (red) from both ventricles.

## 2.2 Distance Regularized Level Set Evolution

In this subsection, we first review the distance regularized level set evolution (DRLSE) model proposed in [18], which is used to perform the preliminary segmentation of the LV and RV, and which is also a basis of our two-level formulation of the proposed level set method in the second step. Let  $I$  be an image on a domain  $\Omega$ , we define an edge indicator function  $g$  by

$$g \triangleq \frac{1}{1+|\nabla G_\delta * I|^2} \quad (1)$$

where  $G_\delta$  is a Gaussian kernel with a standard deviation  $\delta$ . The convolution in ((1)) is used to smooth the image to reduce the noise. This function  $g$  usually takes smaller values at object boundaries than at other locations.

For a level set function (LSF)  $\phi: \Omega \rightarrow R$ , we define an energy functional  $\mathcal{E}(\phi)$  by

$$\mathcal{E}(\phi) = \mu \mathcal{R}_p(\phi) + \lambda \mathcal{L}_g(\phi) + \alpha \mathcal{A}_g(\phi) \quad (2)$$

where  $\mu > 0$ ,  $\lambda > 0$  and  $\alpha \in R$  are the coefficients of the energy functionals  $\mathcal{R}_p(\phi)$ ,  $\mathcal{L}_g(\phi)$  and  $\mathcal{A}_g(\phi)$ , which are defined by

$$\mathcal{R}_p(\phi) \triangleq \int_\Omega p(|\nabla \phi|) dx \quad (3)$$

$$\mathcal{L}_g(\phi) \triangleq \int_\Omega g \delta(\phi) |\nabla \phi| dx \quad (4)$$

and

$$\mathcal{A}_g(\phi) \triangleq \int_{\Omega} gH(-\phi) dx \quad (5)$$

where  $p$  is a potential function  $p: [0, \infty) \rightarrow R$ , and  $H$ ,  $\delta$  are the Heaviside function and Dirac delta function, respectively. A simple and straightforward definition of the potential  $p$  for distance regularization is defined as

$$p = p_1(s) \triangleq \frac{1}{2}(s - 1)^2 \quad (6)$$

which has  $s = 1$  as the unique minimum point. With this potential  $p = p_1(s)$ , the level set regularization term  $\mathcal{R}_p(\phi)$  can be explicitly expressed as

$$\mathcal{P}(\phi) = \frac{1}{2} \int_{\Omega} (|\nabla\phi| - 1)^2 dx \quad (7)$$

which characterizes the deviation of  $\phi$  from a signed distance function.

A preferable potential function  $p$  for the distance regularization term  $\mathcal{R}_p$  is a double-well potential. Here, we provide a specific construction of the double-well potential  $p_2(s)$  as

$$p_2(s) = \begin{cases} \frac{1}{(2\pi)^2} (1 - \cos(2\pi s)), & \text{if } s \leq 1 \\ \frac{1}{2}(s - 1)^2, & \text{if } s \geq 1. \end{cases} \quad (8)$$

This potential  $p_2(s)$  has two minimum points at  $s = 0$  and  $s = 1$ . It is easy to verify that  $p_2$  is twice differentiable in  $[0, \infty)$ , with the first and second derivatives given by

$$p'_2(s) = \begin{cases} \frac{1}{2\pi} \sin(2\pi s), & \text{if } s \leq 1 \\ s - 1, & \text{if } s \geq 1 \end{cases} \quad (9)$$

and

$$p''_2(s) = \begin{cases} \cos(2\pi s), & \text{if } s \leq 1 \\ 1, & \text{if } s \geq 1. \end{cases} \quad (10)$$

It is easy to verify that the function

$$d_p(s) = p'_2(s)/s \quad (11)$$

satisfies

$$|d_p(s)| < 1, \quad \text{for all } s \in (0, \infty) \quad (12)$$

and

$$\lim_{s \rightarrow 0} d_p(s) = \lim_{s \rightarrow \infty} d_p(s) = 1. \quad (13)$$

Therefore, we have

$$|\mu d_p(|\nabla\phi|)| \leq \mu \quad (14)$$

which verifies the boundedness of the diffusion rate for the potential  $p = p_2$ .

### 2.3 Distance Regularized Two-Level-Set Evolution Model

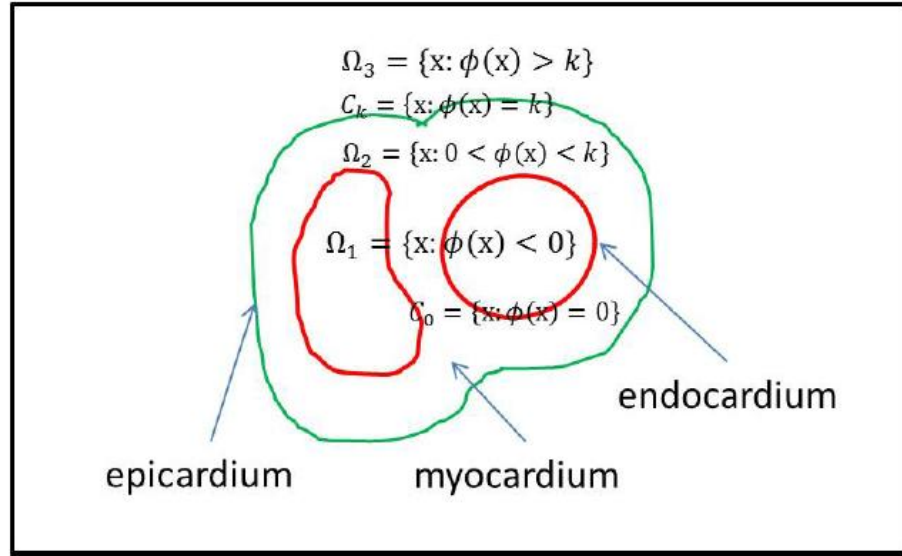


Figure 2: The level set representation of endocardium and epicardium as proposed in the proposed method.

We formulate the segmentation of both ventricles as an optimal problem of seeking for a level set function such that its 0-level and  $k$ -level contours best fit the epicardial and endocardial contours respectively inside the images as shown in Figure 2. Furthermore, according to the anatomical properties of endocardium and epicardium, as discussed in section 2.1, the two-level-set function should satisfy the following two properties: first the 0-level and  $k$ -level contours are smooth, and second the distance between the 0-level and  $k$ -level contours is smoothly changing. Therefore, we propose an extended framework with an energy functional in the following form:

$$F(\phi) = D(\phi) + L(\phi) + A(\phi) \quad (15)$$

where  $L(\phi)$  is an energy functional defined from edge-based image information, such that it is minimized when the 0-level and  $k$ -level contours of the function  $\phi$  are on the endocardium and epicardium;  $A(\phi)$  is weighted area term and introduced to speed up the motion of the 0-level and  $k$ -level contour in the level set evolution process;  $D(\phi)$  is the distance regularization term defined as:

$$D(\phi) = \mu \int (|\nabla\phi| - \alpha)^2 dx \quad (16)$$

where  $\alpha$  is a constant. This distance regularization term is introduced to force the  $|\nabla\phi|$  to be close to a constant, and therefore ensures that the distance between the 0-level and  $k$ -level contours is close to a constant. The constant  $\alpha$  should be approximately equal to  $k/d$ , where  $d$  is the average thickness of the myocardium (in pixel) in the image. Note that this distance regularization term serves as a soft constraint to force  $|\nabla\phi|$  to be close to the constant  $\alpha$ , but not exactly a constant. As a result of this soft constraint,  $|\nabla\phi|$  is smoothly varying, and the distance between the 0-level and  $k$ -level contours is smoothly varying. In this paper, we allowed the level set function  $\phi$  take positive values inside the 0-level contour  $C_0$  and negative values outside  $C_0$ .

The energy  $L$  contour is defined by,

$$L(\phi) = \int g[\lambda_1\delta(\phi) + \lambda_2\delta(\phi - k)]|\nabla\phi|dx \quad (17)$$

where  $g$  is an edge indicator function, which is defined as,

$$g \triangleq \frac{1}{1+|\nabla G_{\sigma} * I|}. \quad (18)$$

The above defined energy  $L(\phi)$  computes the line integral of the function  $g$  along the 0-level and  $k$ -level contours. Obviously, this energy is minimized when the 0-level and  $k$ -level contours of the level set function  $\phi$  are located on desired object boundaries, where the function  $g$  takes smaller values than other non-edge locations. The weighted area term is defined by,

$$A(\phi) = \alpha_0 \int gH(-\phi)dx + \alpha_k \int gH(-\phi + k)dx \quad (19)$$

The minimization of the energy  $A_g$  is achieved by shrinking and expanding the 0-level and  $k$ -level contours, depending on the sign of  $\alpha_0$  and  $\alpha_k$  of the banded region between the 0-level and  $k$ -level contour when they arrive at object boundaries where take larger values.

## 2.4 Energy Minimization

With the energy terms including  $L(\phi)$ ,  $A(\phi)$  and  $D(\phi)$  defined above, we propose to minimize the following energy functional:

$$F(\phi) = L(\phi) + A(\phi) + D(\phi). \quad (20)$$

This energy functional can be minimized by alternately minimizing  $F$  with respect to each of its variables. The energy minimization process starts with an initialization of the level set function  $\phi$  and the smooth function  $\alpha$ . We minimise the function  $F$  with respect to  $\phi$  applying gradient flow method and get,

$$\begin{aligned} \frac{\partial \phi}{\partial t} &= -\frac{\partial E}{\partial \phi} \\ &= \operatorname{div} \left( g \frac{\nabla \phi}{|\nabla \phi|} \right) [\lambda_1 \delta(\phi) + \lambda_2 \delta(\phi - k)] \\ &\quad + \partial g [\delta(\phi - k) - \delta(\phi)] + \mu \left( \nabla^2 \phi - \alpha \operatorname{div} \left( \frac{\nabla \phi}{|\nabla \phi|} \right) \right) \end{aligned} \quad (21)$$

In practice, the Heaviside function  $H$  is approximated by the following smooth function  $H_\varepsilon$  defined as

$$H_\varepsilon(y) = \begin{cases} \frac{1}{2} \left[ 1 + \frac{y}{\varepsilon} + \frac{1}{\pi} \sin \left( \frac{\pi y}{\varepsilon} \right) \right], & \text{if } |x| \leq \varepsilon \\ 1, & \text{if } x > \varepsilon \\ 0, & \text{if } x < -\varepsilon \end{cases} \quad (22)$$

and  $\delta_\varepsilon$  is the derivative of  $H_\varepsilon$  as

$$\delta_\varepsilon(y) = \begin{cases} \frac{1}{2\varepsilon} \left[ 1 + \cos \left( \frac{\pi y}{\varepsilon} \right) \right], & \text{if } |x| \leq \varepsilon \\ 0, & \text{if } |x| > \varepsilon. \end{cases} \quad (23)$$

### 3 Implementation with Two Steps

In this section, we describe a two-step approach for segmentation of LV and RV. In the first step, we use the DRLSE to perform a preliminary segmentation of LV and RV to roughly locate the endocardial contours of the LV and RV. The level set function obtained in the first step is used as the initial level set function of the proposed level set evolution in [18] in the second step, with the 0-level and  $k$ -level contours representing the initial endocardial and epicardial contours, respectively. The final endocardial and epicardial contours of LV and RV are then obtained as the result of the level set evolution in the proposed model described in Section 2.3 and 2.4. The details of this two-step approach are described below.

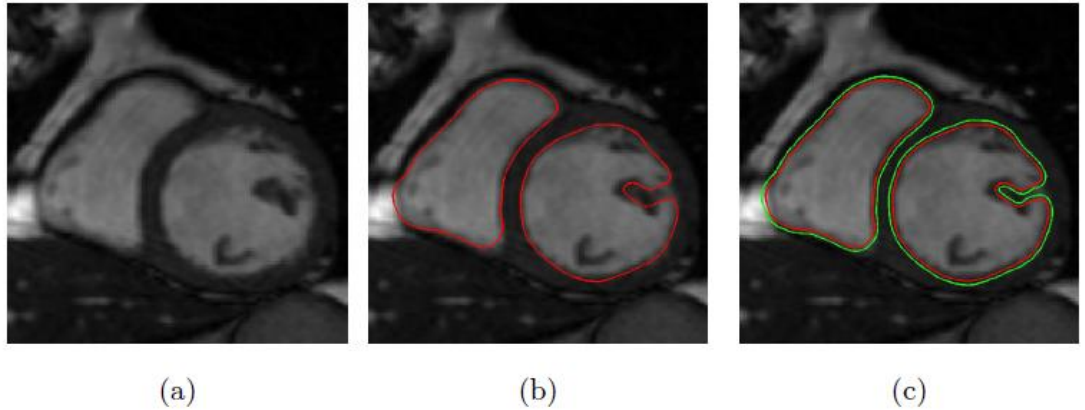


Figure 3: Roughly locate endocardial contours of LV and RV using distance regularized level set evolution (DRLSE) model: (a) initialization for DRLSE, (b) final zero level of DRLSE used as the initialization of two-level-set function, (c) initialization of two-level-set-function.

#### 3.1 Preliminary Segmentation of LV and RV Using DRLSE

In the first step, we use distance regularized level set evolution (DRLSE) model to obtain a preliminary segmentation of left and right ventricles, which is then applied to define the initial level set function for the distance regularized two-level-set model described in Section 2.

Figure 3 illustrates the complete process of preliminary segmentation from cardiac images, which includes manual initialization as well as final contours resulted from the DRLSE model, respectively. First, we place two square blocks inside cavities of the left and the right ventricle for the initialization of the DRLSE model. Then the final zero level contour in DRLSE is evolved to capture the inner contours of both LV and RV. The final contours of the DRLSE model are going to be used as the initial endocardial contours in the following segmentation step. Given the segmented left and right ventricles obtained in the first step, denoted by  $V_{left}$  and  $V_{right}$ , we constructed the initial level set function for the second step as:

$$\phi_0(x) = \begin{cases} c & x \in V_{left} \cup V_{right} \\ -c & else \end{cases} \quad (24)$$

where  $c$  is a positive constant.

### 3.2 Extraction of Both Endocardial and Epicardial Contours Using Proposed Model

The second step of our method aims to accurately capture both the endocardial contours as well as the epicardial contours of both LV and RV at the same time, based on the previously initialized results. In this step, we incorporate the anatomical knowledge of the heart as shown in Figure 1 into our two-level-set formulation, where the endocardial and epicardial contours are represented by two specified level contours from one level set function. With the above two-level-set representation of endocardial and epicardial contours, we implement the mathematical model discussed in Section 2 to accurately segment left and right ventricles from cine-MRI based on previously initialized contours from DRLSE method.

In details, the preliminary segmentation of inner contours of left and right ventricles from DRLSE as well as selected different level contours from the same level set function are used to initialize the endocardial contour and the epicardial contour separately in proposed model, which are labeled as the 0-level contour and the  $k$ -level contour. Both level sets are optimized by an energy minimization process as proposed in Section 2.4 to best estimate the actual endocardium and epicardium of LV and RV from cardiac images. In the following section, we are going to demonstrate the implementation details as well as the segmentation results from the proposed two-step method.

## 4 Experimental Results

In this section, we demonstrate the implementation details as well as the segmentation results of the proposed two-step approach with the application to segment left and right ventricles using cardiac cine-MRI data derived from MICCAI 2009 left ventricular segmentation challenge, the MICCAI 2012 right ventricular segmentation challenge and the MICCAI 2013 challenge workshop.

### 4.1 Parameters Selection

In first step, we set the parameters for the DRLSE model with  $\Delta t = 1$ ,  $\mu = 0.2$ , and  $\lambda = 10$ . In the second step, we numerically solve the level set evolution equation of proposed model presented in Eq. (15) by following a standard finite difference scheme proposed in [18]. The details of the selected parameters for the proposed model are provided. Time step  $\Delta t$  used in the approximation of temporal derivative was set to  $\Delta t = 0.1$  in our implementation. For the datasets used in this paper, remaining parameters were  $\alpha_0 = -3$ ,  $\alpha_k = -3$ ,  $\rho = 3$ ,  $\mu = 1$ ,  $\omega = 0.5$ ,  $\lambda_1 = 1$ ,  $\lambda_2 = 1$ . The choice of the level  $k = 140$ . As mentioned earlier, the constant  $\alpha$  should be approximately equal to  $k/d$ , where  $d$  is the average thickness of the myocardium (in pixel) in the image. From the images in the dataset used in our work, we know the average thickness of the myocardium is 10 in pixel. Therefore, we chose  $\alpha = 140/10 = 14$ .

## 4.2 Segmentation Results

### 4.2.1 Results for MICCAI 2009 challenge on left ventricle segmentation and MICCAI 2013 challenge workshop

Our two-step approach has been tested on the dataset of MICCAI 2009 challenge on left ventricle segmentation ([http://smial.sri.utoronto.ca/LV\\_Challenge/Home.html](http://smial.sri.utoronto.ca/LV_Challenge/Home.html)) and MICCAI 2013 challenge workshop ([https://masi.vuse.vanderbilt.edu/workshop2013/index.php/Main\\_Page](https://masi.vuse.vanderbilt.edu/workshop2013/index.php/Main_Page)). We first show our left ventricle segmentation result for one CMR image named DET0001101 from MICCAI 2013 challenge workshop as an example in Figure 4. In MICCAI 2009 left ventricle segmentation challenge, the metrics for quantitative evaluation included average perpendicular distance (APD) and the Dice similarity coefficient (DSC) where DSC is a measure of the overlap of two regions and is defined by

$$DSC = \frac{2 \times |A \cap B|}{|A| + |B|} \quad (25)$$

where  $|*|$  is the area of region \*. The MICCAI challenge evaluation criterion grades a detected contour as good if the APD between ground truth and detected contour is less than 5mm. The quotient formed by dividing the number of detected contours by the number of contours from the ground truth is termed the *detected percentage*. Dividing the number of good contours by the number of detected contours yields the *good percentage*. The results of our proposed method in terms of these metrics are reported in Table 1 for each image case in validation datasets. In [20], [36], [13], [6], APD values and DSC values for validation dataset are reported. We compared the APD and DSC metrics of our segmentation results with the results of methods in [20], [36], [13], [6] as shown in Table 1 shows how the the DSC statistics of our method are not dissimilar to those obtained by other methods in the validation datasets, but our APD values are the smallest suggesting that our contours are closest to the ground truth. Furthermore, we have obtained the highest detected percentage (100%) and highest good percentage for both endocardial (endo) and epicardial (epi) contours in the validation datasets.

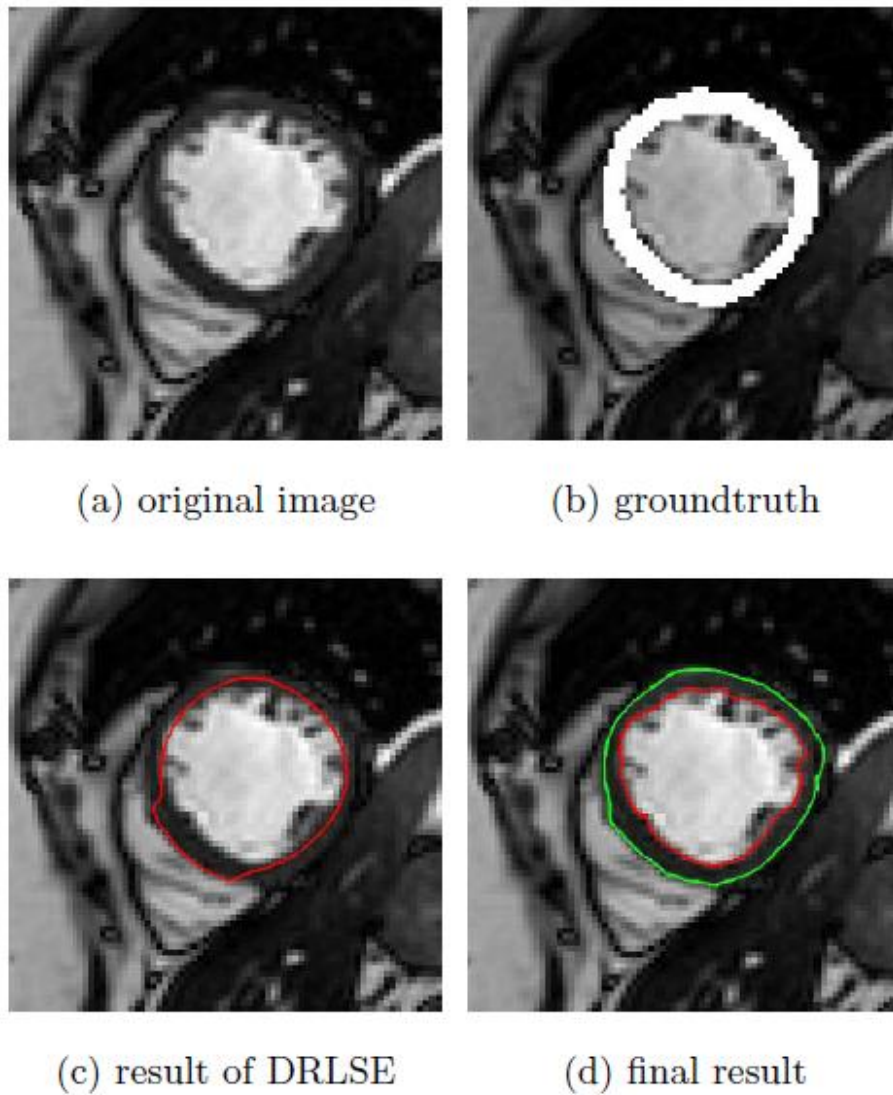


Figure 4: Example of segmentation result from MICCAI 2013 challenge workshop training set(DET0001101); (a)original image, (b)groundtruth, (c)result of DRLSE, (d)final result.

Table 1: Results on validation dataset for the MICCAI 2009 challenge

Patient	Detected (%)		Good (%)		APD (mm)		DSC	
	endo	epi	endo	epi	endo	epi	endo	epi
I-5	SC-HF-	100	100	100	1.15	0.98	0.95	0.97
I-6	SC-HF-	100	100	100	1.27	1.31	0.94	0.96
I-7	SC-HF-	100	100	100	2.23	1.45	0.89	0.95
I-8	SC-HF-	100	100	100	1.83	1.89	0.92	0.95
NI-11	SC-HF-	100	100	100	2.07	1.42	0.91	0.95
NI-31	SC-HF-	100	100	100	1.80	1.80	0.91	0.94
NI-33	SC-HF-	100	100	100	1.98	1.88	0.88	0.92
NI-7	SC-HF-	100	100	100	2.35	1.24	0.91	0.96
P-37	SC-HY	100	100	100	1.41	1.80	0.89	0.94
P-6	SC-HY	100	100	100	1.44	2.21	0.91	0.92
P-7	SC-HY	100	100	75	2.30	1.67	0.88	0.95
P-8	SC-HY	100	100	89.47	2.14	2.09	0.88	0.94
SC-N-5	SC-N-5	100	100	93.33	2.14	1.48	0.82	0.94
SC-N-6	SC-N-6	100	100	100	2.10	1.39	0.87	0.95
SC-N-7	SC-N-7	100	100	100	1.26	1.25	0.91	0.94

Table 2: Left ventricle segmentation results of different methods for 2009 LV MICCAI validation data sets

group	[20]	[36]	[13]	[6]	our method
APD(mm)(%)endo	2.07±0.61	2.29±0.57	2.04±0.47	2.44±0.62	1.76±0.57
APD(mm)(%)epi	1.91±0.63	2.28±0.39	2.35±0.57	2.05±0.59	1.95±0.43
DSC(%)endo	0.89±0.03	0.89±0.03	0.89±0.04	0.88±0.03	0.95±0.01
DSC(%)epi	0.94±0.02	0.93±0.01	0.92±0.02	0.93±0.02	0.92±0.03
detected(%)endo	77.78±17.35	99.7±1.4	100	-	100
detected(%)epi	85.68±14.06	100	100	-	100
good(%)endo	72.45±19.52	86.4±11	94.33±9.93	92.28±6.05	97.83±0.21
good(%)epi	81.11±13.95	94.2±7.0	95.6±6.90	92.22±5.02	97.48±0.33

‘-’ means no value reported in this paper.

#### 4.2.2 Results for MICCAI 2012 right ventricle segmentation challenge

Our two-step approach has been additionally tested on the dataset of MICCAI 2012 right ventricle segmentation challenge (<http://www.litislab.eu/rvsc>).

Figure 5 illustrates segmentation results of left and right ventricles from a randomly selected patient cine-MRI using the proposed method after applying DRLSE initialization. Each of these figures corresponds to one of the middle steps within the iteration (iterates from left to right and from top to bottom). The proposed segmentation model accurately captures the endocardial and epicardial contour detail in both left and right ventricles, even in the presence of intensity inhomogeneity and image noise (refer to bottom right panel in Figure 5). Figure 6 shows the results and ground truth for subject P15 in the training set. We selected two slices at end-diastole and end-systole and achieved promising results using our proposed method.

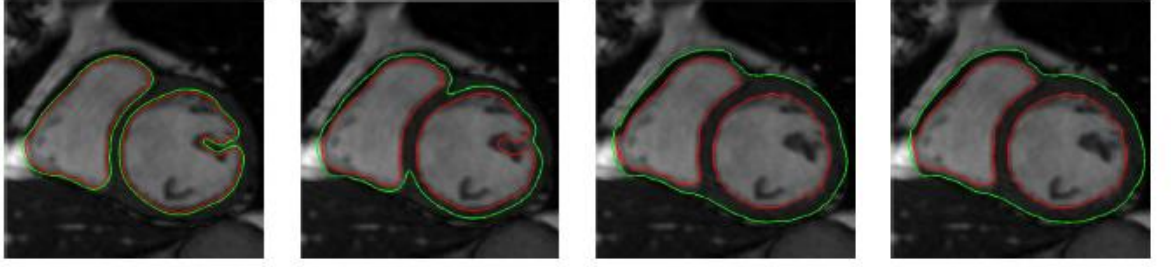
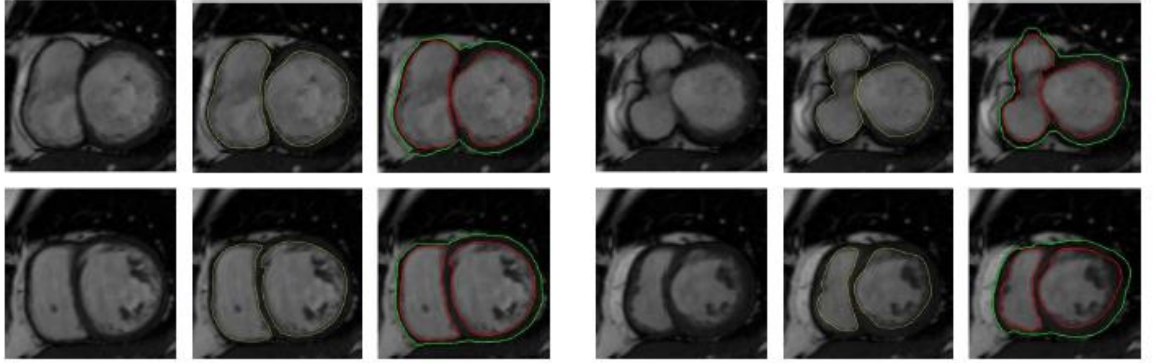


Figure 5: Evolution of the 0-level and  $k$ -level contours in the proposed distance regularized two-level-set model, starting from the initial contours (on the left) obtained in the first step as shown in Figure 3c.



(a) End-diastole

(b) End-systole

Figure 6: Results of our method (right column) and ground truth (middle column) for the images (left column) at end-diastole shown in (a) and end-systole in (b). Each row shows one of two slices in the images from one case.

Table 3 compares our segmentation results to others using datasets from the MICCAI 2012 right ventricle segmentation challenge using DSC and Hausdorff distance (HD) metrics. HD provides a symmetric distance measure of the maximal discrepancy between two labeled contours and is defined as,

$$HD(A, B) = \max \left( \max_{a \in A} (\min_{b \in B} d(a, b)), \max_{b \in B} (\min_{a \in A} d(a, b)) \right) \quad (26)$$

where  $d(a, b)$  denotes Euclidean distance. ED and ES stand for end-diastole and end-systole, respectively. Table 3 shows promising results for our method compared to the other three methods.

Table 3: Right ventricle segmentation results of different methods for 2012 RV MICCAI test1 data sets

2*	[43]		[21]		[33]		our method	
	ED	ES	ED	ES	ED	ES	ED	ES
*En	DM 17)	0.83(0. 27)	0.72(0. 11)	0.86(0. 25)	0.88(0. 11)	0.77(0. 15)	0.90(0. 23)	0.82(0. 23)
	HD 88)	9.77(7. 0.49)	11.41(1 74)	7.70(3. .53)	11.16(5 03)	7.69(6. .69)	10.71(7 47)	7.51(5. .03)
*Ep	DM 13)	0.86(0. 23)	0.77(0. 08)	0.88(0. 17)	0.77(0. 08)	0.90(0. 13)	0.82(0, 21)	0.89(0. 57)
	HD 22)	10.23(7 .46)	11.81(9 72)	7.93(3. .44)	11.72(5 96)	8.02(5. .70)	11.52(7 19)	9.36(8. .03)

ACCEPTED MANUSCRIPT

## 5 Conclusions

In this paper, we present a new segmentation method for left and right ventricles from cardiac MR short-axis images. This framework contains two steps: firstly we apply the DRLSE method as initialization of endocardial contour and then we use the two-level-set model to accurately capture both endocardial and epicardial contours for LV and RV, simultaneously. Experimental results have demonstrated the effectiveness of this proposed two-step level set approach for segmenting cardiac left and right ventricles from cine-MRI. Quantitative evaluation and comparison with some state-of-the-art methods show advantage of our method in terms of segmentation accuracy.

## References

- [1] Ismail Ben Ayed, Hua-mei Chen, Kumaradevan Punithakumar, Ian Ross, and Shuo Li. Max-flow segmentation of the left ventricle by recovering subject-specific distributions via a bound of the bhattacharyya measure. *Medical image analysis*, 16(1):87–100, 2012.
- [2] Wenjia Bai, Wenzhe Shi, D.P. O’Regan, Tong Tong, Haiyan Wang, S. Jamil-Copley, N.S. Peters, and D. Rueckert. A probabilistic patch-based label fusion model for multi-atlas segmentation with registration refinement: Application to cardiac mr images. *Medical Imaging, IEEE Transactions on*, 32(7):1302–1315, July 2013.
- [3] O. Bruder, A. Wagner, M. Lombardi, J. Schwitter, van Rossum A, G. Pilz, D. Nothnagel, H. Steen, S. Petersen, E. Nagel, S. Prasad, J. Schumm, S. Greulich, A. Cagnolo, P. Monney, C. C. Deluigi, T. Dill, H. Frank, G. Sabin, S. Schneider, and H. Mahrholdt. European cardiovascular magnetic resonance (eurocmr) registry–multi national results from 57 centers in 15 countries. *J Cardiovasc Magn Reson*, 18(15:9), 2013.
- [4] T.F. Chan and L.A. Vese. Active contours without edges. *Image Processing, IEEE Transactions on*, 10(2):266–277, 2001.
- [5] Yunmei Chen, Hemant D. Tagare, Sheshadri Thiruvankadam, Feng Huang, David Wilson, Kaundinya S. Gopinath, Richard, W. Briggs, and Edward A. Geiser. Using prior shapes in geometric active contours in a variational framework. *IJCV*, 50:315–328, 2002.
- [6] C. Constantinides, Y. Chenoune, N. Kachenoura, E. Rouillot, E. Mousseaux, A. Herment, and F. Frouin. Semi-automated cardiac segmentation on cine magnetic resonance images using GVF-Snake deformable models. *MIDAS J-Card MR Left Ventricle Segmentation Challenge*, 2009.
- [7] L. Dornheim, K. D. Tonnie, and K. Dixon. Automatic segmentation of the left ventricle in 3D SPECT data by registration with a dynamic anatomic model. *Med Image Comput Comput Assist Interv (MICCAI)*, 8(Pt 1):335–342, 2005.
- [8] UK Biobank Elliott P, Peakman TC. The uk biobank sample handling and storage protocol for the collection, processing and archiving of human blood and urine. *Int J Epidemiol*, 37(2):234–44, 2008.

- [9] A. F. Frangi, W. J. Niessen, and M. A. Viergever. Three-dimensional modelling for functional analysis of cardiac images: a review. *IEEE Trans Med Imag*, 20(1):2–5, 2001.
- [10] Huaifei Hu, Haihua Liu, Zhiyong Gao, and Lu Huang. Hybrid segmentation of left ventricle in cardiac mri using gaussian-mixture model and region restricted dynamic programming. *Magnetic resonance imaging*, 31(4):575–584, 2013.
- [11] K. Jaspers, H. G. Freling, van Wijk K, E. I. Romijn, M. J. Greuter, and T. P. Willems. Improving the reproducibility of mr-derived left ventricular volume and function measurements with a semi-automatic threshold-based segmentation algorithm. *Int J Cardiovasc Imaging*, 29(3):617–623, 2013.
- [12] M.P. Jolly. Automatic segmentation of the left ventricle in cardiac MR and CT images. *Inter J Comput Vis*, 70(2):151–163, 2006.
- [13] M. P. Jolly. Fully automatic left ventricle segmentation in cardiac cine MR images using registration and minimum surfaces. *MIDAS J-Card MR Left Ventricle Segmentation Challenge*, 2009.
- [14] Michael Kass, Andrew Witkin, and Demetri Terzopoulos. Snakes: Active contour models. *International Journal of Computer Vision*, 1(4):321–331, 1988.
- [15] S. Kirschbaum, J. P. Aben, T. Baks, A. Moelkerand K. Gruszczynska, G. P. Krestin, W. J. van der Giessen, D. J. Duncker, P. J. de Feyter, and R. J. van Geuns. Accurate automatic papillary muscle identification for quantitative left ventricle mass measurements in cardiac magnetic resonance imaging. *Acad Radiol*, 15(10):1227–1233, 2008.
- [16] U. Kurkure, A. Pednekar, R. Muthupillai, S. D. Flamm, and I. A. Kakadiaris. Localization and segmentation of left ventricle in cardiac cine-MR images. *IEEE Trans Biomed Eng*, 56(5):1360–1370, 2009.
- [17] M.E. Leventon, W.E.L. Grimson, and O. Faugeras. Statistical shape influence in geodesic active contours. In *Computer Vision and Pattern Recognition, 2000. Proceedings. IEEE Conference on*, volume 1, pages 316–323 vol.1, 2000.

[18] C. Li, C. Xu, C. Gui, and M. D. Fox. Distance regularized level set evolution and its application to image segmentation. *IEEE Trans Image Processing*, 19(12):3243–3254, 2010.

[19] M. Lorenzo-Valdés, G. I. Sanchez-Ortiz, A. G. Elkington, R. H. Mohiaddin, and D. Rueckert. Segmentation of 4D cardiac MR images using a probabilistic atlas and the EM algorithm. *Med Image Anal*, 8(3):255–265, 2004.

[20] Y. Lu, P. Radau, K. Connelly, A. Dick, and G. Wright. Automatic image-driven segmentation of left ventricle in cardiac cine MRI. *MIDAS J-Card MR Left Ventricle Segmentation Challenge*, 2009.

[21] Michael Lynch, Ovidiu Ghita, and Paul F Whelan. Left-ventricle myocardium segmentation using a coupled level-set with a priori knowledge. *Computerized Medical Imaging and Graphics*, 30(4):255–262, 2006.

[22] R. Malladi, J.A. Sethian, and B.C. Vemuri. Shape modeling with front propagation: a level set approach. *Pattern Analysis and Machine Intelligence, IEEE Transactions on*, 17(2):158–175, Feb 1995.

[23] Meng Ma, Marijn van Stralen, Johan HC Reiber, Johan G Bosch, and Boudewijn PF Lelieveldt. Model driven quantification of left ventricular function from sparse single-beat 3d echocardiography. *Medical image analysis*, 14(4):582–593, 2010.

[24] Chuang Miao. Comparative studies of different system models for iterative ct image reconstruction. *Dissertations & Theses - Gradworks*, 2013.

[25] Chuang Miao. Compressive sensing based image reconstruction for computed tomography dose reduction. *Dissertations & Theses - Gradworks*, 2015.

[26] C. Miao and H. Yu. A general-thresholding solution for regularized ct reconstruction. *Image Processing IEEE Transactions on*, 24(12):5455–5468, 2015.

[27] J. Montagnat, M. Sermesant, H. Delingette, G. Malandain, and N. Ayache. Anisotropic filtering for model-based segmentation of 4D cylindrical echocardiographic images. *Pattern Recognition Letters*, 24(4-5):815–828, 2003.

- [28] N. Paragios. A variational approach for the segmentation of the left ventricle in cardiac image analysis. *Int J Comput Vis*, 50(3):345–362, 2002.
- [29] C. Petitjean and J. N. Dacher. A review of segmentation methods in short axis cardiac MR images. *Med Image Anal*, 15(2):169–184, 2011.
- [30] Xiaohua Qian, Yuan Lin, Yue Zhao, Jing Wang, Jing Liu, and Xiahai Zhuang. Segmentation of myocardium from cardiac mr images using a novel dynamic programming based segmentation method. *Medical Physics*, 42(3):1424–1435, 2015.
- [31] Xiaohua Qian, Jiahui Wang, Shuxu Guo, and Qiang Li. An active contour model for medical image segmentation with application to brain ct image. *Medical Physics*, 40(2), December 2012.
- [32] S. Queirós, D. Barbosa, B. Heyde, P. Morais, J. L. Vila-Ás, D. Friboulet, O. Bernard, and J. Dâ€™hooge. Fast automatic myocardial segmentation in 4d cine cmr datasets. *Med Image Anal*, 18(7):1115–1131, 2014.
- [33] Jordan Ringenberg, Makarand Deo, Vijay Devabhaktuni, Omer Berenfeld, Pamela Boyers, and Jeffrey Gold. Fast, accurate, and fully automatic segmentation of the right ventricle in short-axis cardiac {MRI}. *Computerized Medical Imaging and Graphics*, 38(3):190 – 201, 2014.
- [34] B. D. Rosen, T. Edvardsen, S. Lai, E. Castillo, L. Pan, Jerosch-Herold M, S. Sinha, R. Kronmal, D. Arnett, Crouse JR 3rd, S. R. Heckbert, D. A. Bluemke, and J. A. Lima. Left ventricular concentric remodeling is associated with decreased global and regional systolic function: the multi-ethnic study of atherosclerosis. *Circulation*, 112(7):984–91, 2008.
- [35] B. Sievers, S. Kirchberg, A. Bakan, U. Franken, and H. J. Trappe. Impact of papillary muscles in ventricular volume and ejection fraction assessment by cardiovascular magnetic resonance. *J Cardiovasc Magn Reson*, 6(1):9–16, 2004.
- [36] J. Wijnhout, D. Hendriksen, H. Van Assen, and R. Van der Geest. LV challenge LKEB contribution: fully automated myocardial contour detection. *MIDAS J-Card MR Left Ventricle Segmentation Challenge*, 2009.

- [37] Jia Wu and John C Brigham. Computational techniques for analysis of shape and kinematics of biological structures. In *Image-Based Geometric Modeling and Mesh Generation*, pages 251–269. Springer, 2013.
- [38] Jia Wu, Katharine G Brigham, Marc A Simon, and John C Brigham. An implementation of independent component analysis for 3d statistical shape analysis. *Biomedical Signal Processing and Control*, 13:345–356, 2014.
- [39] Jia Wu, Yingqian Wang, Marc A Simon, and John C Brigham. A new approach to kinematic feature extraction from the human right ventricle for classification of hypertension: a feasibility study. *Physics in medicine and biology*, 57(23):7905, 2012.
- [40] X. Zeng, L. H. Staib, R. T. Schultz, and J. S. Duncan. Volumetric layer segmentation using coupled surfaces propagation. In *IEEE Conference on Computer Vision and Pattern Recognition (CVPR)*, pages 708–715, 1998.
- [41] Honghai Zhang, Andreas Wahle, Ryan K Johnson, Thomas D Scholz, and Milan Sonka. 4-d cardiac mr image analysis: left and right ventricular morphology and function. *Medical Imaging, IEEE Transactions on*, 29(2):350–364, 2010.
- [42] Shaohua Kevin Zhou. Shape regression machine and efficient segmentation of left ventricle endocardium from 2d b-mode echocardiogram. *Medical Image Analysis*, 14(4):563–581, 2010.
- [43] Ourselin S Zuluaga MA, Cardoso MJ. Automatic right ventricle segmentation using multi-label fusion in cardiac mri. *Medical Image Computing and Computer-Assisted Intervention, Workshop on RV Segmentation Challenge in Cardiac MRI*, 2012.